Supporting Information: Q-Band Relaxation in Chlorophyll: New Insights from Multireference Quantum Dynamics

Sebastian Reiter,[†,¶] Lena Bäuml,[†,¶] Jürgen Hauer,[‡] and Regina de Vivie-Riedle[*,†]

†*Department of Chemistry, Ludwig-Maximilians-Universität München, Butenandtstr. 11, 81377 Munich, Germany*

‡*Department of Chemistry, Technical University of Munich, Lichtenbergstr. 4, 85747 Garching, Germany*

¶*Contributed equally to this work*

E-mail: regina.de_vivie@cup.uni-muenchen.de

Contents

1 Influence of the Phytyl Chain

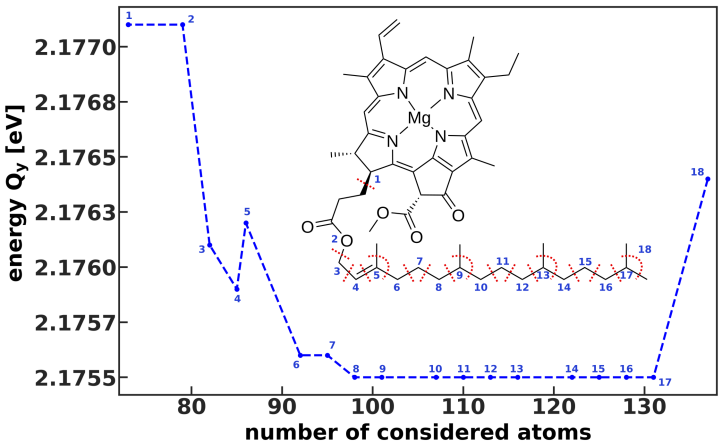

Figure S1: Absorption energy of Q_y for different lengths of the phytyl chain. Red lines indicate the cut bonds that were saturated with hydrogen atoms for each data point.

2 Benchmarks of Multireference Calculations

2.1 Active Space Size and Composition

We tested three active spaces ranging from the (6,6) space shown in the main manuscript over (8,8) and (10,10) to (22,22), whose compositions are shown in figs. S2 to S4 respectively. Absolute energies along with the characters of the leading configurations of the first six roots are listed in table S1. Excitation energies relative to the ground state are compiled in table S2.

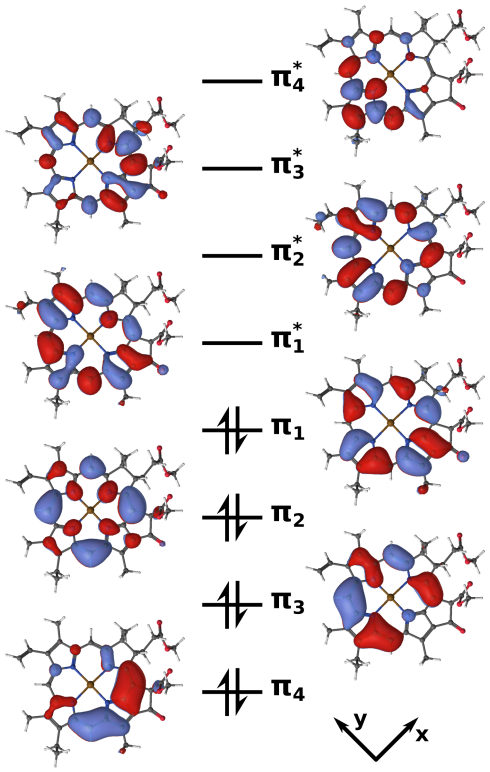

Figure S2: Active space for the XMS-CASPT2(8,8) calculation.

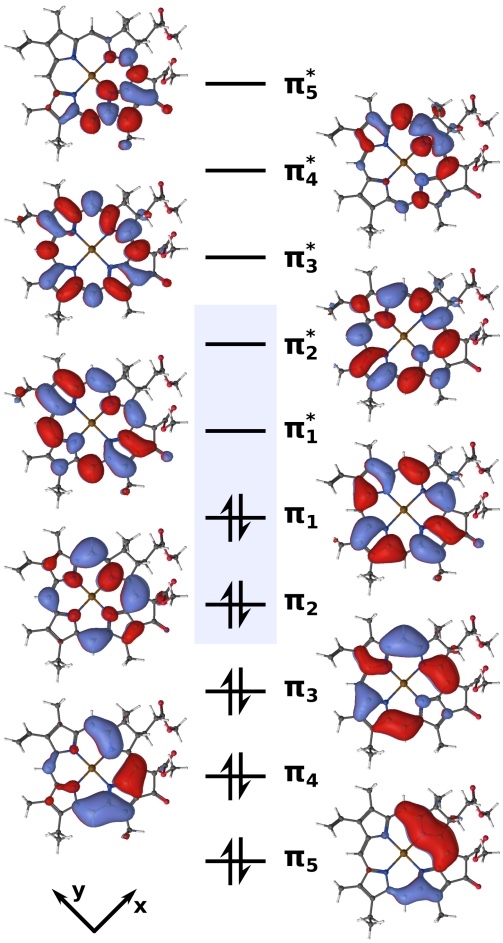

Figure S3: Active space for the XMS-CASPT2(10,10) calculation.

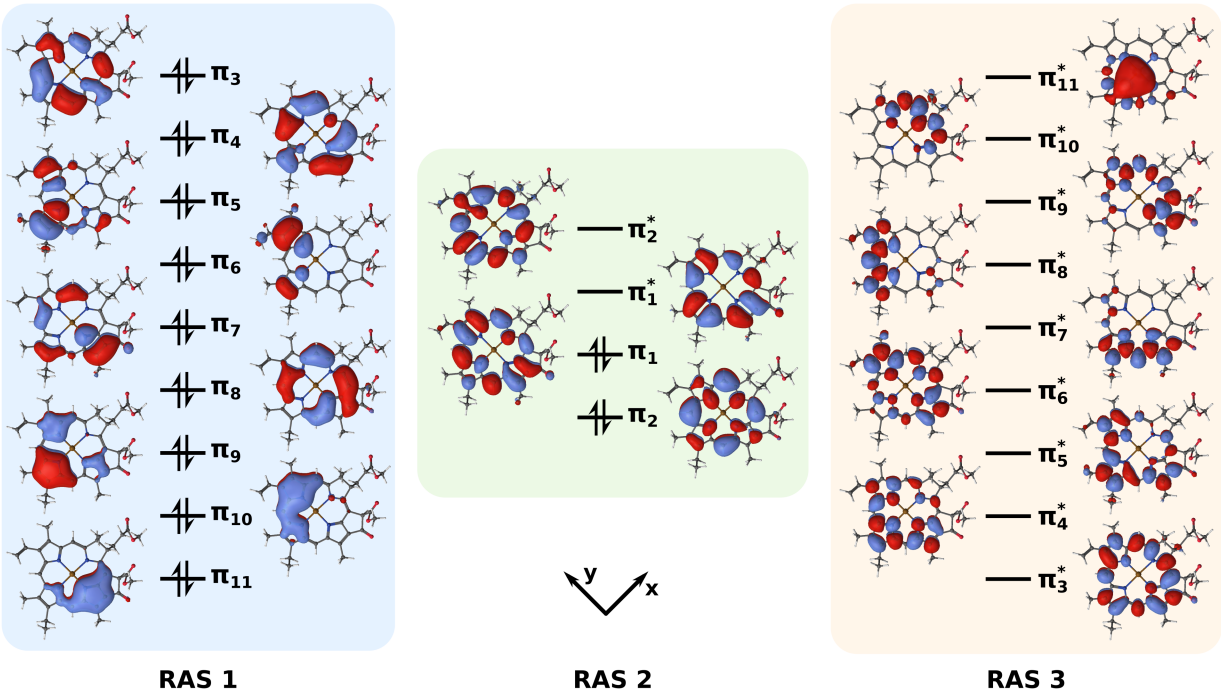

Figure S4: Active space for the MS-RASPT2(22,1,1;9,4,9) and MS-RASPT2(22,2,2;9,4,9) calculations. The notation refers to 22 electrons in the active space, where the subspaces RAS 1, RAS 2 and RAS 3 contain 9, 4 and 9 orbitals, respectively and single or double excitations are allowed from RAS 1 or into RAS 3. All excitations are allowed between the four Gouterman orbitals in RAS 2. State-averaging and MS-CASPT2 was performed over six roots.

Table S1: Energies (E_h) and leading CI coefficients of the first six roots of a chlorophyll a model with different active spaces. State-averaging was performed over six roots and an IPEA-shift of 0.25 and an imaginary shift of 0.1 was applied for all of the CASPT2 calculations in these tests.

method	root 1	root 2	root 3
XMS-CASPT2(6,6)	-2184.71470585	-2184.61666043	-2184.60533006
	(GS, $c = -0.93651$)	($\pi_1 \rightarrow \pi_1^*$, $c = -0.72107$)	($\pi_2 \rightarrow \pi_1^*$, $c = -0.66005$)
XMS-CASPT2(8,8)	-2184.70700256	-2184.61015970	-2184.59043254
	(GS, $c = 0.924095$)	($\pi_1 \rightarrow \pi_1^*$, $c = 0.857211$)	($\pi_1 \rightarrow \pi_2^*$, $c = 0.631309$)
XMS-CASPT2(10,10)	-2184.70445539	-2184.60738802	-2184.59273935
	(GS, $c = -0.913262$)	($\pi_1 \rightarrow \pi*_1$, $c = 0.749743$)	($\pi_2 \rightarrow \pi_1^*$, $c = -0.691811$)
MS-RASPT2(22,9,9;22,1,1)	-2184.60360263	-2184.51769497	-2184.50286833
	(GS, $c = -0.903649$)	($\pi_1 \rightarrow \pi_1^*$, $c = -0.824469$)	($\pi_2 \rightarrow \pi_1^*$, $c = 0.732545$)
MS-RASPT2(22,9,9;22,2,2)	-2184.67589339	-2184.58995682	-2184.57484134
	(GS, $c = 0.868498$)	($\pi_1 \rightarrow \pi_1^*$, $c = 0.818706$)	($\pi_2 \rightarrow \pi_1^*$, $c = -0.723248$)

method	root 4	root 5	root 6
XMS-CASPT2(6,6)	-2184.56908121	-2184.56256371	-2184.53758146
	($\pi_1, \pi_1 \rightarrow \pi_1^*, \pi_1^*$, $c = -0.46428$)	($\pi_1 \rightarrow \pi_2^*$, $c = 0.46540$)	($\pi_2 \rightarrow \pi_2^*$, $c = 0.44586$)
XMS-CASPT2(8,8)	-2184.54966707	-2184.54543501	-2184.53235822
	($\pi_2 \rightarrow \pi_1^*$, $c = 0.432443$)	($\pi_2, \pi_1 \rightarrow \pi_1^*, \pi_1^*$, $c = -0.451272$)	($\pi_1, \pi_1 \rightarrow \pi_1^*, \pi_1^*$, $c = -0.593435$)
XMS-CASPT2(10,10)	-2184.55523511	-2184.54431714	-2184.51378096
	($\pi_1 \rightarrow \pi_2^*$, $c = -0.415712$)	($\pi_2, \pi_1 \rightarrow \pi_1^*, \pi_1^*$, $c = 0.492806$)	($\pi_1, \pi_1 \rightarrow \pi_2^*, \pi_2^*$, $c = -0.421454$)
MS-RASPT2(22,9,9;22,1,1)	-2184.47897065	-2184.45661819	-2184.45085734
	($\pi_1 \rightarrow \pi_2^*$, $c = 0.649248$)	($\pi_2, \pi_1 \rightarrow \pi_1^*, \pi_1^*$, $c = -0.602604$)	($\pi_1, \pi_1 \rightarrow \pi_1^*, \pi_1^*$, $c = -0.622145$)
MS-RASPT2(22,9,9;22,2,2)	-2184.54673920	-2184.52908185	-2184.51453413
	($\pi_1 \rightarrow \pi_2^*$, $c = 0.701008$)	($\pi_2 \rightarrow \pi_2^*$, $c = -0.672110$)	($\pi_1, \pi_1 \rightarrow \pi_1^*, \pi_1^*$, $c = 0.736266$)

Table S2: Relative energies (eV) of the first six roots of a chlorophyll *a* model with different active spaces. State-averaging was performed over six roots and an IPEA-shift of 0.25 and an imaginary shift of 0.1 was applied for all of the CASPT2 calculations in these tests.

method	root 1	root 2	root 3	root 4	root 5	root 6	$\lvert Q_x - Q_y \rvert$
XMS-CASPT2(6,6)	0.00	2.67	2.98	3.96	4.14	4.82	0.31
XMS-CASPT2(8,8)	0.00	2.64	3.17	4.28	4.40	4.75	0.54
XMS-CASPT2(10,10)	0.00	2.64	3.04	4.06	4.36	5.19	0.40
MS-RASPT2(22,9,9;22,1,1)	0.00	2.34	2.74	3.39	4.00	4.16	0.40
MS-RASPT2(22,9,9;22,2,2)	0.00	2.34	2.75	3.51	3.99	4.39	0.41

2.2 IPEA and Imaginary Shifts

2.2.1 SA6-CASSCF(6,6) → XMS-CASPT2

Table S3: Absolute energies (E_h) of the first six roots of a chlorophyll a model with different level shifts at the SA6-CASSCF(6,6)/XMS-CASPT2 level of theory.

IPEA	Imag.	root 1	root 2	root 3
0.00	0.00	−2184.72415897	−2184.68837625	−2184.66185535
		(GS, $c = -0.93243$)	($\pi_3 \to \pi_1^*$, $c = 0.484950$)	($\pi_1 \to \pi_1^*$, $c = -0.60471$)
0.00	0.20	−2184.72357950	−2184.65485037	−2184.64811020
		(GS, $c = 0.929222$)	($\pi_1 \to \pi_1^*$, $c = 0.67156$)	($\pi_2 \to \pi_1^*$, $c = -0.658412$)
0.00*	0.25	−2184.70320053	−2184.64673205	−2184.64043692
		(GS, $c = -0.940482$)	($\pi_2 \to \pi_1^*$, $c = 0.76015$)	($\pi_1 \to \pi_1^*$, $c = -0.750108$)
0.10	0.00	−2184.71931571	−2184.63846089	−2184.63266879
		(GS, $c = -0.94338$)	($\pi_1 \to \pi_1^*$, $c = 0.67764$)	($\pi_2 \to \pi_1^*$, $c = -0.64904$)
0.10	0.10	−2184.71941552	−2184.63881306	−2184.63113895
		(GS, $c = 0.94128$)	($\pi_1 \to \pi_1^*$, $c = 0.69624$)	($\pi_2 \to \pi_1^*$, $c = -0.66757$)
0.10	0.20	−2184.71917171	−2184.63677155	−2184.62745227
		(GS, $c = 0.93992$)	($\pi_1 \to \pi_1^*$, $c = 0.71317$)	($\pi_2 \to \pi_1^*$, $c = -0.68969$)
0.25	0.00	−2184.71474167	−2184.61984561	−2184.61147716
		(GS, $c = -0.93753$)	($\pi_1 \to \pi_1^*$, $c = -0.73191$)	($\pi_2 \to \pi_1^*$, $c = -0.71099$)
0.25*	0.00	−2184.69708086	−2184.60978223	−2184.60289128
		(GS, $c = -0.94543$)	($\pi_1 \to \pi_1^*$, $c = -0.71319$)	($\pi_2 \to \pi_1^*$, $c = 0.64882$)
0.25	0.10	−2184.71470585	−2184.61666043	−2184.60533006
		(GS, $c = -0.93651$)	($\pi_1 \to \pi_1^*$, $c = -0.72107$)	($\pi_2 \to \pi_1^*$, $c = -0.66005$)
0.25	0.20	−2184.71437778	−2184.61529367	−2184.60262515
		(GS, $c = -0.94705$)	($\pi_1 \to \pi_1^*$, $c = -0.75842$)	($\pi_2 \to \pi_1^*$, $c = -0.71745$)

IPEA	Imag.	root 4	root 5	root 6
0.00	0.00	−2184.65556601	−2184.64057694	−2184.60326590
		($\pi_2 \to \pi_1^*$, $c = -0.53992$)	($\pi_2 \to \pi_1^*$, $c = -0.61788$)	($\pi_2 \to \pi_2^*$, $c = 0.50952$)
0.00	0.20	−2184.61864975	−2184.61611037	−2184.57877185
		($\pi_1 \to \pi_2^*$, $c = -0.48719$)	($\pi_1 \to \pi_1^*$, $c = -0.46075$)	($\pi_3 \to \pi_1^*$, $c = 0.43852$)
0.00*	0.25	−2184.61363127	−2184.59984056	−2184.56787402
		($\pi_1 \to \pi_2^*$, $c = -0.76884$)	($\pi_1 \to \pi_1^*$, $c = -0.35516$)	($\pi_3 \to \pi_1^*$, $c = 0.42617$)
0.10	0.00	−2184.60972278	−2184.59464721	−2184.51971137
		($\pi_1 \to \pi_2^*$, $c = -0.60871$)	($\pi_2 \to \pi_2^*$, $c = 0.54855$)	($\pi_3 \to \pi_1^*$, $c = 0.42951$)
0.10	0.10	−2184.59808455	−2184.59026492	−2184.56688608
		($\pi_1 \to \pi_2^*$, $c = -0.51967$)	($\pi_2 \to \pi_2^*$, $c = 0.45384$)	($\pi_3 \to \pi_1^*$, $c = 0.44241$)
0.10	0.20	−2184.59297865	−2184.58657928	−2184.56172721
		($\pi_1 \to \pi_2^*$, $c = -0.47851$)	($\pi_1 \to \pi_2^*$, $c = 0.40944$)	($\pi_3 \to \pi_1^*$, $c = 0.44333$)
0.25	0.00	−2184.57627155	−2184.57019047	−2184.48928302
		($\pi_1 \to \pi_2^*$, $c = -0.62402$)	($\pi_2 \to \pi_2^*$, $c = 0.52480$)	($\pi_1, \pi_3 \to \pi_1^*$, $c = -0.42205$)
0.25*	0.00	−2184.56989501	−2184.55840357	−2184.53805303
		($\pi_1 \to \pi_2^*$, $c = -0.81041$)	($\pi_2 \to \pi_2^*$, $c = 0.65376$)	($\pi_1, \pi_1 \to \pi_1^*, \pi_1^*$, $c = -0.65947$)
0.25	0.10	−2184.56908121	−2184.56256371	−2184.53758146
		($\pi_1, \pi_1 \to \pi_1^*, \pi_1^*$, $c = -0.46428$)	($\pi_1 \to \pi_2^*$, $c = 0.46540$)	($\pi_2 \to \pi_2^*$, $c = 0.44586$)
0.25	0.20	−2184.56489745	−2184.55956086	−2184.53305906
		($\pi_1 \to \pi_2^*$, $c = -0.48709$)	($\pi_2 \to \pi_2^*$, $c = 0.43731$)	($\pi_3 \to \pi_1^*$, $c = 0.44839$)

* using a different initial guess for the CASSCF reference wave function than in the final calculations

Table S4: Relative energies (eV) of the first six roots of a chlorophyll a model with different level shifts at the SA6-CASSCF(6,6)/XMS-CASPT2 level of theory.

IPEA	Imag.	root 1	root 2	root 3	root 4	root 5	root 6	$\lvert Q_x - Q_y \rvert$
0.00	0.00	0.00	0.97	1.70	1.87	2.27	3.29	0.17
0.00	0.20	0.00	1.87	2.05	2.90	3.12	3.71	0.18
0.00*	0.25	0.00	1.54	1.71	2.44	2.81	3.68	0.17
0.10	0.00	0.00	2.20	2.36	2.98	3.39	5.43	0.16
0.10	0.10	0.00	2.19	2.40	3.30	3.51	4.15	0.21
0.10	0.20	0.00	2.24	2.50	3.43	3.61	4.28	0.26
0.25	0.00	0.00	2.58	2.81	3.77	3.93	6.14	0.23
0.25*	0.00	0.00	2.38	2.56	3.46	3.77	4.33	0.19
0.25	0.10	0.00	2.67	2.98	3.96	4.14	4.82	0.31
0.25	0.20	0.00	2.70	3.04	4.07	4.21	4.93	0.34

* using a different initial guess for the CASSCF reference wave function than in the final calculations

2.2.2 SA4-CASSCF(6,6) → SA6-CASCI(6,6) → XMS-CASPT2

Table S5: Absolute energies (E_h) of the first six roots of a chlorophyll a model with different level shifts at the SA4-CASSCF(6,6)/SA6-CASCI(6,6)/XMS-CASPT2 level of theory.

IPEA	Imag.	root 1	root 2	root 3
0.050	0.10	−2184.71793960	−2184.64018158	−2184.62653499
		(GS, $c = -0.93753$)	($\pi_1 \to \pi_1^*$, $c = -0.79503$)	($\pi_1 \to \pi_2^*$, $c = -0.55267$)
0.050	0.20	−2184.71766209	−2184.63706507	−2184.62067806
		(GS, $c = -0.93647$)	($\pi_1 \to \pi_1^*$, $c = -0.79760$)	($\pi_1 \to \pi_2^*$, $c = -0.54207$)
0.075	0.10	−2184.71701182	−2184.63621309	−2184.62216611
		(GS, $c = -0.93922$)	($\pi_1 \to \pi_1^*$, $c = -0.79500$)	($\pi_1 \to \pi_2^*$, $c = -0.561300$)
0.075	0.20	−2184.71672682	−2184.63330339	−2184.61663781
		(GS, $c = -0.93813$)	($\pi_1 \to \pi_1^*$, $c = -0.79919$)	($\pi_1 \to \pi_2^*$, $c = -0.54851$)
0.090	0.10	−2184.71648245	−2184.63392440	−2184.61966932
		(GS, $c = -0.94009$)	($\pi_1 \to \pi_1^*$, $c = -0.79554$)	($\pi_1 \to \pi_2^*$, $c = -0.566230$)
0.100	0.05	−2184.71604283	−2184.63363367	−2184.62223400
		(GS, $c = -0.94087$)	($\pi_1 \to \pi_1^*$, $c = -0.78024$)	($\pi_1 \to \pi_2^*$, $c = -0.58293$)
0.100	0.10	−2184.71613840	−2184.63242966	−2184.61804552
		(GS, $c = -0.92310$)	($\pi_1 \to \pi_1^*$, $c = -0.79606$)	($\pi_2 \to \pi_1^*$, $c = -0.56940$)
0.110	0.10	−2184.71580053	−2184.63095715	−2184.61645026
		(GS, $c = -0.94113$)	($\pi_1 \to \pi_1^*$, $c = -0.79667$)	($\pi_1 \to \pi_2^*$, $c = -0.57247$)

IPEA	Imag.	root 4	root 5	root 6
0.050	0.10	−2184.60477428	−2184.59165420	−2184.56801483
		($\pi_2 \to \pi_1^*$, $c = -0.61690$)	($\pi_3 \to \pi_1^*$, $c = 0.42687$)	($\pi_1, \pi_3 \to \pi_1^*, \pi_2^*$, $c = 0.37865$)
0.050	0.20	−2184.59748854	−2184.58378493	−2184.56208042
		($\pi_2 \to \pi_1^*$, $c = -0.62284$)	($\pi_3 \to \pi_1^*$, $c = 0.45322$)	($\pi_1, \pi_3 \to \pi_1^*, \pi_2^*$, $c = 0.38504$)
0.075	0.10	−2184.59998473	−2184.58604449	−2184.56204673
		($\pi_2 \to \pi_1^*$, $c = -0.60622$)	($\pi_3 \to \pi_1^*$, $c = 0.43109$)	($\pi_1, \pi_3 \to \pi_1^*, \pi_2^*$, $c = 0.37899$)
0.075	0.20	−2184.59304068	−2184.57835227	−2184.55645904
		($\pi_2 \to \pi_1^*$, $c = -0.61583$)	($\pi_3 \to \pi_1^*$, $c = 0.45417$)	($\pi_1, \pi_3 \to \pi_1^*, \pi_2^*$, $c = 0.38473$)
0.090	0.10	−2184.59722041	−2184.58279321	−2184.55863474
		($\pi_2 \to \pi_1^*$, $c = -0.60040$)	($\pi_3 \to \pi_1^*$, $c = 0.43301$)	($\pi_1, \pi_3 \to \pi_1^*, \pi_2^*$, $c = 0.37914$)
0.100	0.05	−2184.59929752	−2184.58536777	−2184.55880218
		($\pi_2 \to \pi_1^*$, $c = -0.57222$)	($\pi_1, \pi_1 \to \pi_1^*, \pi_1^*$, $c = -0.42101$)	($\pi_1, \pi_3 \to \pi_1^*, \pi_2^*$, $c = 0.37552$)
0.100	0.10	−2184.59541436	−2184.58066644	−2184.55641846
		($\pi_2 \to \pi_1^*$, $c = -0.59673$)	($\pi_3 \to \pi_1^*$, $c = 0.43412$)	($\pi_1, \pi_3 \to \pi_1^*, \pi_2^*$, $c = 0.37922$)
0.110	0.10	−2184.59363463	−2184.57856959	−2184.55424417
		($\pi_2 \to \pi_1^*$, $c = -0.59321$)	($\pi_3 \to \pi_1^*$, $c = -0.43511$)	($\pi_1, \pi_3 \to \pi_1^*, \pi_2^*$, $c = 0.37928$)

Table S6: Relative energies (eV) of the first six roots of a chlorophyll a model with different level shifts at the SA4-CASSCF(6,6)/SA6-CASCI(6,6)/XMS-CASPT2 level of theory.

IPEA	Imag.	root 1	root 2	root 3	root 4	root 5	root 6	$\lvert Q_x - Q_y \rvert$
0.050	0.10	0.00	2.12	2.49	3.08	3.44	4.08	0.37
0.050	0.20	0.00	2.19	2.64	3.27	3.64	4.23	0.45
0.075	0.10	0.00	2.20	2.58	3.18	3.56	4.22	0.38
0.075	0.20	0.00	2.27	2.72	3.37	3.77	4.36	0.45
0.090	0.10	0.00	2.25	2.36	3.25	3.64	4.30	0.11
0.100	0.05	0.00	2.24	2.55	3.18	3.56	4.28	0.26
0.100	0.10	0.00	2.28	2.67	3.29	3.67	4.35	0.39
0.110	0.10	0.00	2.31	2.70	3.32	3.73	4.40	0.39

3 Optimized Geometries and Coordinate Vectors

Optimized geometries of the ground state, Q_y and Q_x minimum are provided in separate plain-text xyz-files. Coordinate vectors for the non-adiabatic coupling at the Q_y minimum, as well as the five normal modes spanning the investigated 2D spaces are provided in separate plain-text xyz-files. All coordinate vectors are defined as displacements from the Q_y state structure in Angstrom.

4 Energy Levels at Minimum Energy Geometries

Energy levels at the Franck-Condon (FC) point and at the Q_x and Q_y minima were computed at the DFT/MRCI level and are provided in tables S7 and S8. The state ordering is retained upon relaxation from the FC point to either of the excited state minima and the $Q_x - Q_y$ gap remains nearly constant. This indicates that Q_x and Q_y do not cross in an energetically accessible region of space.

Table S7: Absolute energies of S_0, Q_y and Q_x at their respective minimum energy geometries in E_h.

geom	S_0	Q_y	Q_x
S_0-min	−2186.244 712	−2186.172 303	−2186.163 694
Q_y-min	−2186.243 441	−2186.174 430	−2186.163 986
Q_x-min	−2186.243 383	−2186.173 246	−2186.164 254

Table S8: Energy levels of Q_y and Q_x at the Franck-Condon point (FC) and their respective minimum energy geometries. Energies are given in eV, relative to the ground state minimum energy.

geom	S_O	Q_y	Q_x	$\lvert Q_x - Q_y \rvert$
S_0-min	0.00	1.97	2.20	0.23
Q_y-min	0.03	1.91	2.20	0.28
Q_x-min	0.04	1.94	2.19	0.24

5 Potential Energy Surfaces

For the 2D PES spanned by the modes 195/194, 195/198, 195/92 and 195/74 a total of 45 points distributed between $-0.2\,\text{Å}$ and $0.2\,\text{Å}$ have been explicitly calculated. For all four coordinate spaces the Q_y and Q_x PES with the calculated points are visualized in figs. S5 to S8.

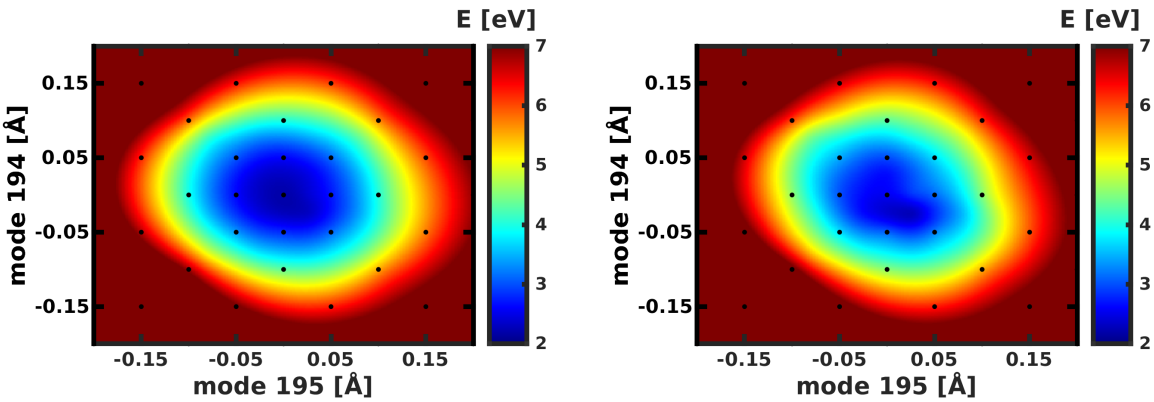

(a) Q_y PES. (b) Q_x PES.

Figure S5: Calculated points (black) for the 2D space spanned by modes 195/194.

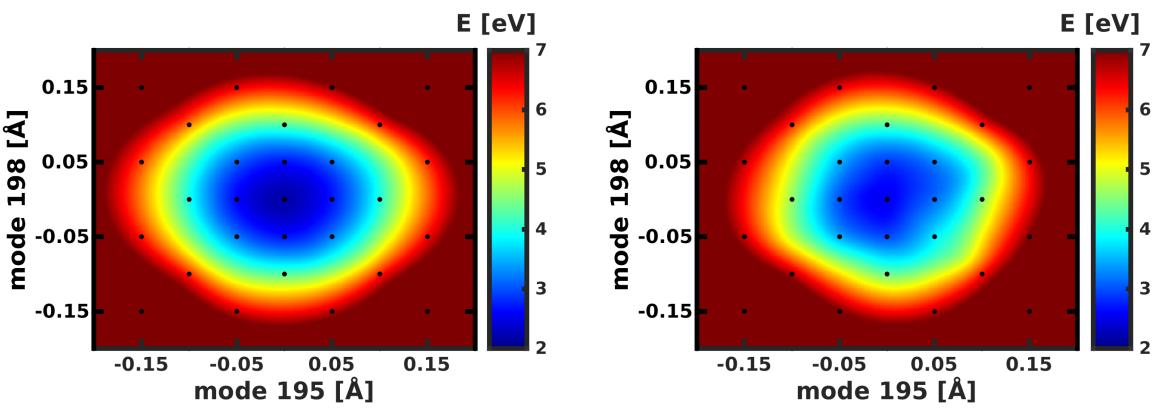

(a) Q_y PES. (b) Q_x PES.

Figure S6: Calculated points (black) for the 2D space spanned by modes 195/198.

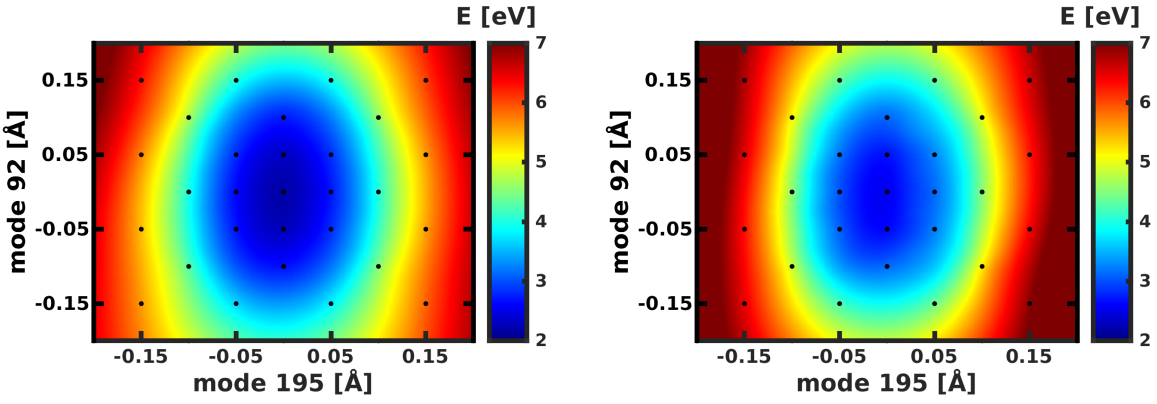

(a) Q_y PES. (b) Q_x PES.

Figure S7: Calculated points (black) for the 2D space spanned by modes 195/92.

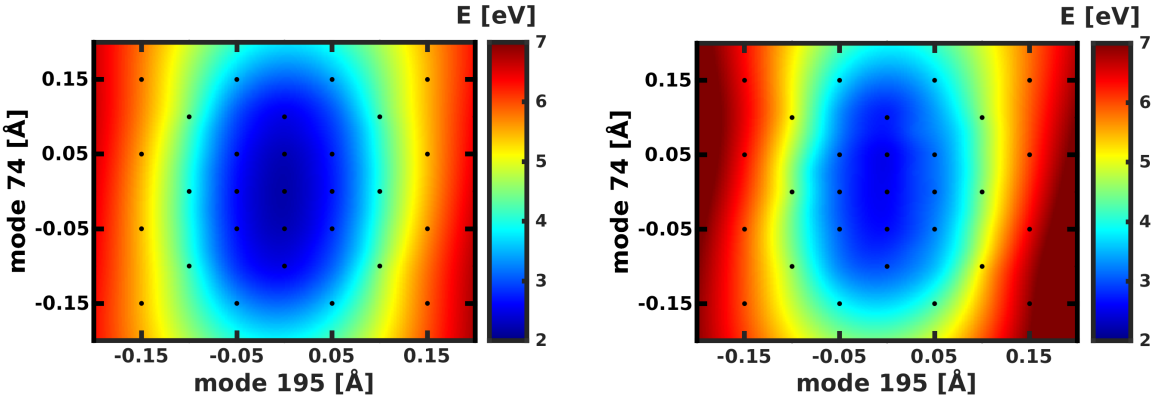

(a) Q_y PES. (b) Q_x PES.

Figure S8: Calculated points (black) for the 2D space spanned by modes 195/74.

6 Non-adiabatic Coupling Matrix Elements

Non-adiabatic coupling matrix elements (NACs) were calculated at the SA4-CASSCF(6,6)/SA6-CASCI(6,6)/ANO-RCC-VDZP level of theory and scaled to the energy difference between CASSCF and XMS-CASPT2 as detailed in the main article. The NACs for coordinate spaces 195/194 and 195/74 are provided in the main article, those for coordinate spaces 195/198 and 195/92 are shown in figs. S9 and S10, respectively.

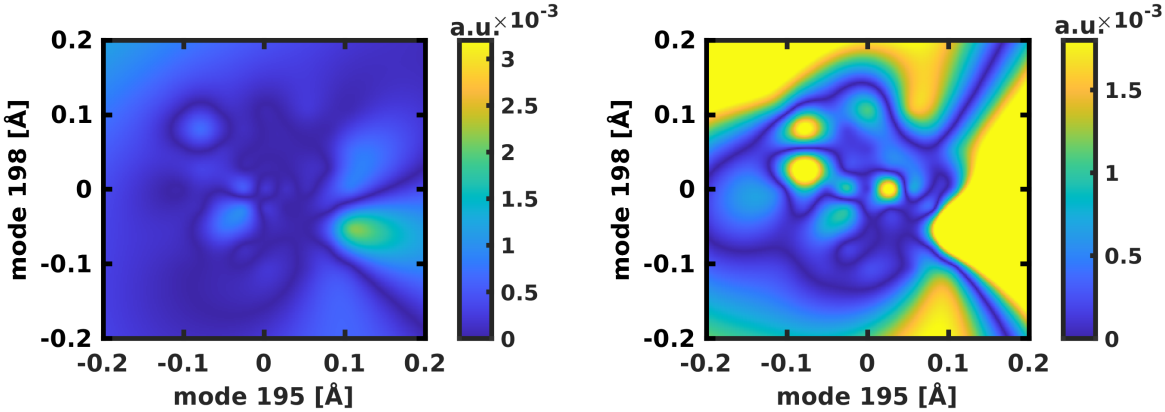

(a) $\left\langle \Psi_1 \left| \frac{\partial}{\partial q_{195}} \right| \Psi_2 \right\rangle$. (b) $\left\langle \Psi_1 \left| \frac{\partial}{\partial q_{198}} \right| \Psi_2 \right\rangle$.

Figure S9: Visualization of the NACs in the coordinate space spanned by modes 195/198, projected onto the two internal coordinates.

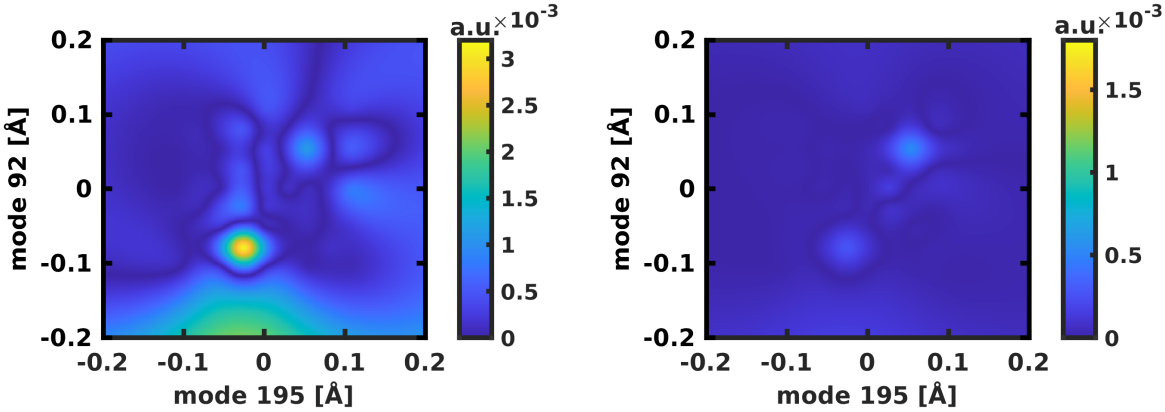

(a) $\left\langle \Psi_1 \left| \frac{\partial}{\partial q_{195}} \right| \Psi_2 \right\rangle$. (b) $\left\langle \Psi_1 \left| \frac{\partial}{\partial q_{92}} \right| \Psi_2 \right\rangle$.

Figure S10: Visualization of the NACs in the coordinate space spanned by modes 195/92, projected onto the two internal coordinates.

7 Transition Dipole Moments

Transition dipole moments for the laser excitation in the coordinate space spanned by modes 195/194 are provided in fig. S11. They were calculated at the SA4-CASSCF(6,6)/SA6-CASCI(6,6)/ANO-RCC-VDZP level of theory as detailed in the main manuscript.

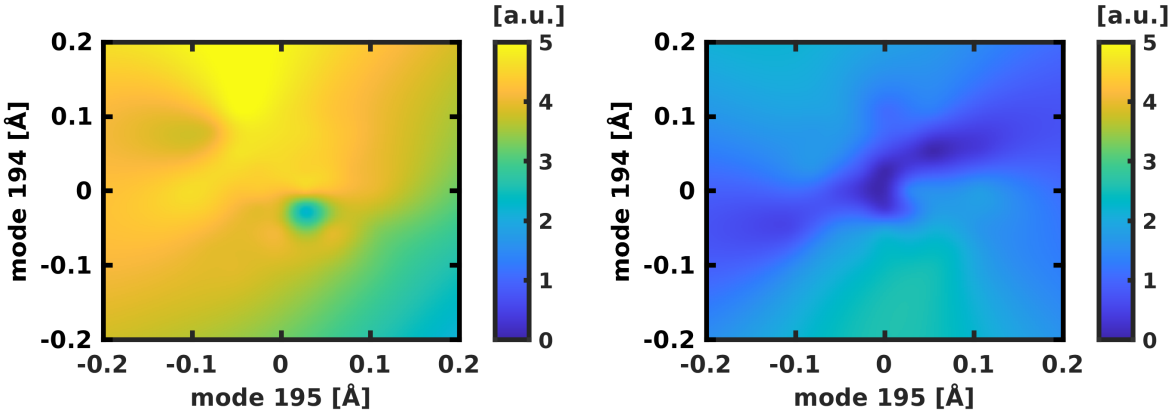

(a) Q_y.

(b) Q_x.

Figure S11: Visualization of the transition dipole moments for the Q_y and Q_x states in the coordinate space spanned by modes 195/194.

8 Quantum Dynamics

The kinetic energy $\hat{T}_q$ in internal coordinates was evaluated in the G-Matrix formalism, where it takes the form:[S1–S4]

$$\hat{T}_q \simeq -\frac{1}{2}\sum_{r=1}^{M}\sum_{s=1}^{M}\frac{\partial}{\partial q_r}\left[G_{rs}\frac{\partial}{\partial q_s}\right]. \tag{1}$$

The G-matrix G_{rs} is defined via the derivative of the internal coordinates q_r with respect to the Cartesian coordinates x_i:

$$G_{rs} = \sum_{i=1}^{3N}\frac{1}{m_i}\frac{\partial q_r}{\partial x_i}\frac{\partial q_s}{\partial x_i} \tag{2}$$

In practice, it is often easier to compute

$$G_{rs}^{-1} = \sum_{i=1}^{3N} m_i \frac{\partial x_i}{\partial q_r}\frac{\partial x_i}{\partial q_s} \tag{3}$$

and subsequently invert the matrix to obtain G_{rs}. As we work with linear coordinate spaces, the G-matrix is constant across each 2D space and its matrix elements are provided in table S9.

Table S9: G-matrix elements for the 2D coordinates spanned by modes 195/198, 195/194, 195/92 and 195/74. G_{11} is the matrix element along mode 195, G_{22} along the respective second mode. G_{12} denotes the kinetic coupling and is numerically zero due to the use of orthogonal coordinates.

modes	G_{11} [a.u.]	G_{12} [a.u.]	G_{22} [a.u.]
195/198	1.3738×10^{-5}	5.3925×10^{-9}	1.3414×10^{-5}
195/194	1.3756×10^{-5}	5.0243×10^{-7}	1.3968×10^{-5}
195/92	1.3758×10^{-5}	5.6629×10^{-7}	1.6214×10^{-5}
195/74	1.3741×10^{-5}	2.2344×10^{-7}	1.6392×10^{-5}

The temporal evolution of the population in the Q_x and Q_y state for the propagation in the 2D coordinate spaces spanned by the modes 195/194, 195/198 and 195/92 respectively are shown in Fig. S12. For the propagation in the 195/92 space a Butterworth filter eliminating all parts of the wave packet below a value of -0.20 Å in y-coordinate was applied.

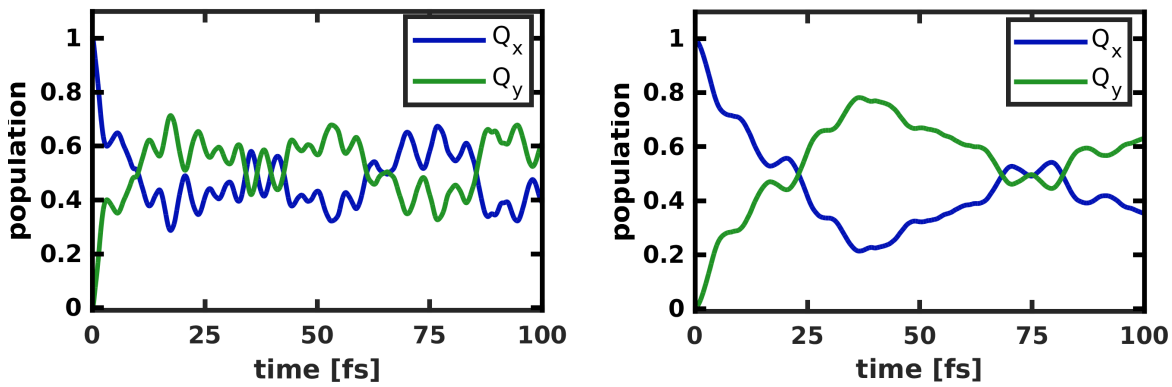

(a) (b)

Figure S12: Temporal evolution of the population for the 2D spaces spanned by a) modes 195/198 and b) modes 195/92.

9 Overlap of Normal Modes with the NAC Vector

This section provides the overlap of each normal mode at the ground state minimum with the non-adiabatic coupling vector (table S10). The modes that contribute the most were used in the construction of a two-dimensional coordinate space for the subsequent non-adiabatic dynamics calculations. The contribution s_i of each normal mode $\mathbf{q}_i$ to the non-adiabatic coupling vector $\mathbf{f}$ was calculated via vector projection in Cartesian coordinates:

$$s_i = \frac{\mathbf{q}_i \cdot \mathbf{f}}{\mathbf{f} \cdot \mathbf{f}}. \tag{4}$$

As the normal modes are orthogonal, the unitless squared quantity s_i^2 provides the percentage of non-adiabatic coupling that is contained in each mode.

Table S10: Overlap of normal modes with the non-adiabatic coupling vector at the Q_y geometry. The harmonic vibrational frequency of each mode is also listed for completeness.

mode	ν **[cm^{-1}]**	**overlap** s_i	**squared overlap** s_i^2
195	1596.31	0.395 261	0.156 232
194	1567.54	0.371 777	0.138 218
198	1642.05	0.289 377	0.083 739
144	1284.59	0.254 025	0.064 529
158	1389.16	0.241 142	0.058 150
159	1407.84	0.209 366	0.043 834
143	1274.23	0.206 716	0.042 732
129	1163.25	0.183 165	0.033 549
171	1479.40	0.177 674	0.031 568
170	1473.23	0.147 845	0.021 858
156	1375.95	0.147 421	0.021 733
130	1171.02	0.143 688	0.020 646
157	1388.23	0.137 688	0.018 958
196	1612.00	0.134 621	0.018 123
109	1015.61	0.131 960	0.017 413
142	1251.78	0.114 548	0.013 121
148	1316.13	0.113 390	0.012 857
197	1632.27	0.108 124	0.011 691
168	1453.43	0.102 603	0.010 527
107	975.02	0.098 366	0.009 676
167	1443.22	0.093 672	0.008 774

Continued on next page

Table S10: Overlap of normal modes with the non-adiabatic coupling vector at the ground state minimum.

mode	ν **[cm^{-1}]**	**overlap** s_i	**squared overlap** s_i^2
183	1512.09	0.088 149	0.007 770
86	768.60	0.087 688	0.007 689
160	1412.24	0.086 562	0.007 493
200	1679.06	0.083 435	0.006 961
199	1665.30	0.081 529	0.006 647
184	1517.02	0.081 074	0.006 573
193	1541.32	0.080 083	0.006 413
169	1469.07	0.079 419	0.006 307
147	1309.61	0.073 326	0.005 377
126	1128.99	0.072 992	0.005 328
93	821.72	0.063 987	0.004 094
131	1171.76	0.060 780	0.003 694
106	967.31	0.060 692	0.003 684
92	817.26	0.060 319	0.003 638
176	1506.08	0.060 132	0.003 616
179	1510.85	0.059 703	0.003 564
81	736.12	0.059 523	0.003 543
65	514.48	0.053 369	0.002 848
104	945.27	0.053 319	0.002 843
115	1067.45	0.052 456	0.002 752
66	550.58	0.050 035	0.002 504
114	1052.15	0.048 816	0.002 383
85	758.93	0.048 680	0.002 370
136	1205.68	0.048 569	0.002 359
172	1483.18	0.048 221	0.002 325
149	1327.09	0.047 823	0.002 287
119	1073.88	0.046 015	0.002 117
70	600.33	0.043 579	0.001 899
162	1426.47	0.043 533	0.001 895
154	1362.02	0.041 235	0.001 700
151	1344.08	0.041 018	0.001 682
177	1508.48	0.040 660	0.001 653
150	1330.66	0.038 525	0.001 484

Continued on next page

Table S10: Overlap of normal modes with the non-adiabatic coupling vector at the ground state minimum.

mode	ν **[cm^{-1}]**	**overlap** s_i	**squared overlap** s_i^2
238	3216.99	0.038 000	0.001 444
89	790.53	0.036 637	0.001 342
192	1536.57	0.035 906	0.001 289
145	1295.17	0.035 465	0.001 258
108	1000.81	0.034 960	0.001 222
79	726.75	0.032 836	0.001 078
163	1434.89	0.032 767	0.001 074
83	747.22	0.032 252	0.001 040
112	1037.16	0.031 903	0.001 018
182	1511.69	0.031 745	0.001 008
103	938.16	0.031 409	0.000 987
88	780.80	0.031 091	0.000 967
201	1724.85	0.030 908	0.000 955
98	877.09	0.028 519	0.000 813
125	1122.01	0.028 455	0.000 810
87	776.27	0.028 060	0.000 787
90	799.80	0.027 419	0.000 752
166	1440.52	0.027 304	0.000 745
141	1239.42	0.027 164	0.000 738
102	930.88	0.026 903	0.000 724
117	1067.77	0.024 631	0.000 607
153	1352.94	0.024 304	0.000 591
51	354.26	0.023 864	0.000 569
124	1102.90	0.023 120	0.000 535
63	495.99	0.022 964	0.000 527
137	1216.68	0.022 411	0.000 502
67	573.82	0.021 934	0.000 481
84	748.71	0.020 901	0.000 437
128	1151.68	0.020 772	0.000 431
120	1076.17	0.020 704	0.000 429
73	656.42	0.020 592	0.000 424
122	1089.97	0.019 891	0.000 396
164	1435.13	0.019 524	0.000 381

Continued on next page

Table S10: Overlap of normal modes with the non-adiabatic coupling vector at the ground state minimum.

mode	ν **[cm^{-1}]**	**overlap** s_i	**squared overlap** s_i^2
116	1067.72	0.019 396	0.000 376
82	743.04	0.018 082	0.000 327
26	153.77	0.017 892	0.000 320
185	1517.77	0.017 857	0.000 319
77	709.00	0.017 749	0.000 315
113	1045.88	0.017 615	0.000 310
202	1819.11	0.017 384	0.000 302
155	1369.07	0.017 331	0.000 300
205	3047.90	0.017 107	0.000 293
161	1418.53	0.017 087	0.000 292
101	893.33	0.016 348	0.000 267
57	416.05	0.016 237	0.000 264
239	3234.13	0.015 979	0.000 255
146	1299.72	0.015 796	0.000 250
64	502.06	0.014 788	0.000 219
78	724.29	0.014 259	0.000 203
110	1026.60	0.014 196	0.000 202
72	644.45	0.013 465	0.000 181
52	361.24	0.013 177	0.000 174
121	1085.42	0.012 946	0.000 168
118	1069.02	0.012 348	0.000 152
61	471.33	0.012 269	0.000 151
186	1519.94	0.012 210	0.000 149
95	847.20	0.011 552	0.000 133
203	1824.07	0.011 290	0.000 127
58	435.23	0.010 897	0.000 119
187	1520.17	0.010 124	0.000 103
18	117.29	0.009 427	0.000 089
237	3201.40	0.008 973	0.000 081
28	172.89	0.008 962	0.000 080
37	226.83	0.008 161	0.000 067
76	691.34	0.008 095	0.000 066
80	734.75	0.007 934	0.000 063

Continued on next page

Table S10: Overlap of normal modes with the non-adiabatic coupling vector at the ground state minimum.

mode	ν **[cm^{-1}]**	**overlap** s_i	**squared overlap** s_i^2
174	1497.48	0.007 799	0.000 061
105	956.83	0.007 753	0.000 060
152	1350.02	0.007 565	0.000 057
211	3063.75	0.007 490	0.000 056
97	859.20	0.007 399	0.000 055
74	669.01	0.007 180	0.000 052
60	450.39	0.006 990	0.000 049
165	1438.01	0.006 962	0.000 048
29	176.90	0.006 477	0.000 042
230	3153.57	0.006 055	0.000 037
48	308.00	0.005 988	0.000 036
49	317.90	0.005 984	0.000 036
50	323.46	0.005 961	0.000 036
39	240.40	0.005 895	0.000 035
33	203.05	0.005 892	0.000 035
231	3153.82	0.005 864	0.000 034
47	302.05	0.005 775	0.000 033
181	1511.40	0.005 749	0.000 033
189	1522.77	0.005 671	0.000 032
34	209.59	0.005 434	0.000 030
45	291.76	0.005 337	0.000 028
111	1032.24	0.005 332	0.000 028
55	385.18	0.005 211	0.000 027
32	196.32	0.005 169	0.000 027
127	1142.25	0.005 139	0.000 026
132	1181.27	0.004 994	0.000 025
46	297.38	0.004 984	0.000 025
139	1230.91	0.004 878	0.000 024
100	892.35	0.004 773	0.000 023
75	684.16	0.004 680	0.000 022
207	3056.11	0.004 534	0.000 021
20	125.49	0.004 389	0.000 019
31	194.28	0.004 382	0.000 019

Continued on next page

Table S10: Overlap of normal modes with the non-adiabatic coupling vector at the ground state minimum.

mode	ν **[cm^{-1}]**	**overlap** s_i	**squared overlap** s_i^2
43	275.05	0.004 371	0.000 019
173	1495.11	0.004 152	0.000 017
135	1199.31	0.003 888	0.000 015
99	889.41	0.003 637	0.000 013
9	57.33	0.003 580	0.000 013
225	3132.20	0.003 167	0.000 010
42	265.00	0.003 027	0.000 009
25	148.22	0.003 004	0.000 009
188	1522.19	0.002 993	0.000 009
91	804.02	0.002 884	0.000 008
36	217.95	0.002 853	0.000 008
190	1523.41	0.002 838	0.000 008
54	378.80	0.002 782	0.000 008
35	212.05	0.002 735	0.000 007
56	388.37	0.002 679	0.000 007
138	1227.93	0.002 644	0.000 007
68	586.51	0.002 633	0.000 007
210	3059.79	0.002 601	0.000 007
17	108.15	0.002 587	0.000 007
175	1498.66	0.002 517	0.000 006
40	251.27	0.002 516	0.000 006
11	65.60	0.002 411	0.000 006
23	136.82	0.002 291	0.000 005
234	3167.21	0.002 232	0.000 005
96	858.22	0.002 199	0.000 005
140	1231.01	0.002 195	0.000 005
71	634.14	0.002 177	0.000 005
38	236.85	0.002 024	0.000 004
180	1510.92	0.002 006	0.000 004
3	21.39	0.001 960	0.000 004
227	3141.58	0.001 906	0.000 004
204	1849.67	0.001 828	0.000 003
1	12.57	0.001 780	0.000 003

Continued on next page

Table S10: Overlap of normal modes with the non-adiabatic coupling vector at the ground state minimum.

mode	ν **[cm^{-1}]**	**overlap** s_i	**squared overlap** s_i^2
240	3249.15	0.001 719	0.000 003
2	17.76	0.001 692	0.000 003
30	178.85	0.001 635	0.000 003
228	3143.18	0.001 633	0.000 003
5	29.11	0.001 599	0.000 003
19	119.96	0.001 571	0.000 002
41	256.29	0.001 534	0.000 002
226	3134.71	0.001 337	0.000 002
22	135.87	0.001 308	0.000 002
53	375.56	0.001 219	0.000 001
44	285.49	0.001 138	0.000 001
212	3074.03	0.001 135	0.000 001
134	1197.08	0.001 103	0.000 001
12	70.40	0.001 088	0.000 001
10	59.49	0.001 038	0.000 001
123	1099.51	0.001 034	0.000 001
8	49.73	0.001 026	0.000 001
223	3127.08	0.001 018	0.000 001
221	3107.98	0.000 988	0.000 001
208	3057.40	0.000 896	0.000 001
220	3103.89	0.000 875	0.000 001
178	1510.33	0.000 762	0.000 001
7	47.43	0.000 735	0.000 001
209	3058.09	0.000 732	0.000 001
62	485.74	0.000 715	0.000 001
191	1525.14	0.000 664	0.000 000
14	84.68	0.000 623	0.000 000
215	3085.05	0.000 617	0.000 000
216	3093.37	0.000 615	0.000 000
133	1195.89	0.000 583	0.000 000
24	145.01	0.000 561	0.000 000
217	3095.41	0.000 516	0.000 000
59	437.65	0.000 430	0.000 000

Continued on next page

Table S10: Overlap of normal modes with the non-adiabatic coupling vector at the ground state minimum.

mode	ν **[cm^{-1}]**	**overlap** s_i	**squared overlap** s_i^2
21	129.69	0.000 421	0.000 000
218	3095.64	0.000 400	0.000 000
27	156.96	0.000 395	0.000 000
94	836.91	0.000 394	0.000 000
16	100.60	0.000 335	0.000 000
229	3149.82	0.000 334	0.000 000
15	93.62	0.000 284	0.000 000
4	24.66	0.000 263	0.000 000
222	3125.48	0.000 249	0.000 000
214	3083.89	0.000 239	0.000 000
224	3130.92	0.000 201	0.000 000
236	3197.26	0.000 201	0.000 000
219	3099.60	0.000 144	0.000 000
69	589.84	0.000 124	0.000 000
233	3160.83	0.000 079	0.000 000
13	80.48	0.000 075	0.000 000
213	3074.94	0.000 051	0.000 000
235	3193.25	0.000 049	0.000 000
206	3050.51	0.000 022	0.000 000
232	3158.14	0.000 015	0.000 000
6	40.81	0.000 004	0.000 000

10 Sample OpenMolcas Input

A sample input for a CASPT2 calculation with OpenMolcas,[S5,S6] as used in the evaluation of energies and non-adiabatic coupling elements for the potential energy surfaces in this work, is provided in listing 1.

```
>>> export MOLCAS_MEM=40000
>>> export MOLCAS_MOLDEN=OFF

>>> COPY $HOMEDIR/template.JobIph JOBOLD

&GATEWAY
  TITLE= title
  COORD= geom.xyz
  BASIS= ANO-RCC-VDZP
  GROUP= NOSYM
  RICD

&SEWARD
  DoAnalytical

&RASSCF
  JOBIph
  CIRESTART
  EXPERT
  SPIN= 1
  RASSCF= 0 0
  NACTEL= 6
  INACTIVE= 163
  RAS2= 6
  CIROOT= 4 4 1
  MAXORB
  0

>>> COPY $Project.JobIph $HOMEDIR/root4.JobIph

&GRID_IT
 SPARSE
 SELECT
 1:154-179

 &RASSCF
  FILEorb = $HOMEDIR/$Project.RasOrb
  EXPERT
```

```
  SPIN= 1
  RASSCF= 0 0
  NACTEL= 6
  INACTIVE= 163
  RAS2= 6
  CIROOT= 6 6 1
  CIONly
  MAXORB
  0

>>> COPY $Project.JobIph $HOMEDIR/root6.JobIph

&ALASKA
 NAC= 2 3

&CASPT2
  IPEAshift= 0.1
  IMAGinary= 0.1
  MAXIter= 500
  XMULTistate= ALL

>>> COPY $Project.JobMix $HOMEDIR/$Project.JobMix

&RASSI
  HEFF
  CIPR
  TRDI
```

Listing 1: Sample OpenMolcas input for a SA4-CASSCF(6,6)/SA6-CASCI(6,6)/XMS-CASPT2 calculation, including non-adiabatic couplings and transition dipole moments.

References

(S1) Wilson, E. B.; Decius, J. C.; Cross, P. C. *Molecular Vibrations: The Theory of Infrared and Raman Vibrational Spectra*; Dover Publications, 1980.

(S2) Schaad, L. J.; Hu, J. The Schrödinger Equation in Generalized Coordinates. *J. Mol. Struct.: THEOCHEM* **1989**, *185*, 203–215.

(S3) Stare, J.; Balint-Kurti, G. G. Fourier Grid Hamiltonian Method for Solving the Vibrational Schrödinger Equation in Internal Coordinates: Theory and Test Applications. *J. Phys. Chem. A* **2003**, *107*, 7204–7214.

(S4) Kowalewski, M.; Mikosch, J.; Wester, R.; de Vivie-Riedle, R. Nucleophilic Substitution Dynamics: Comparing Wave Packet Calculations with Experiment. *J. Phys. Chem. A* **2014**, *118*, 4661–4669.

(S5) Fdez. Galván, I.; Vacher, M.; Alavi, A.; Angeli, C.; Aquilante, F.; Autschbach, J.; Bao, J. J.; Bokarev, S. I.; Bogdanov, N. A.; Carlson, R. K.; Chibotaru, L. F.; Creutzberg, J.; Dattani, N.; Delcey, M. G.; Dong, S. S.; Dreuw, A.; Freitag, L.; Frutos, L. M.; Gagliardi, L.; Gendron, F.; Giussani, A.; González, L.; Grell, G.; Guo, M.; Hoyer, C. E.; Johansson, M.; Keller, S.; Knecht, S.; Kovačević, G.; Källman, E.; Li Manni, G.; Lundberg, M.; Ma, Y.; Mai, S.; Malhado, J. a. P.; Malmqvist, P. A. k.; Marquetand, P.; Mewes, S. A.; Norell, J.; Olivucci, M.; Oppel, M.; Phung, Q. M.; Pierloot, K.; Plasser, F.; Reiher, M.; Sand, A. M.; Schapiro, I.; Sharma, P.; Stein, C. J.; Sø rensen, L. K.; Truhlar, D. G.; Ugandi, M.; Ungur, L.; Valentini, A.; Vancoillie, S.; Veryazov, V.; Weser, O.; Wesoł owski, T. A.; Widmark, P.-O.; Wouters, S.; Zech, A.; Zobel, J. P.; Lindh, R. OpenMolcas: From Source Code to Insight. *J. Chem. Theory Comput.* **2019**, *15*, 5925–5964.

(S6) Aquilante, F.; Autschbach, J.; Baiardi, A.; Battaglia, S.; Borin, V. A.; Chibotaru, L. F.; Conti, I.; De Vico, L.; Delcey, M.; Fdez. Galván, I.; Ferré, N.; Freitag, L.; Garavelli, M.; Gong, X.; Knecht, S.; Larsson, E. D.; Lindh, R.; Lundberg, M.; Malmqvist, P. A. k.; Nenov, A.; Norell, J.; Odelius, M.; Olivucci, M.; Pedersen, T. B.; Pedraza-González, L.; Phung, Q. M.; Pierloot, K.; Reiher, M.; Schapiro, I.; Segarra-Martí, J.; Segatta, F.; Seijo, L.; Sen, S.; Sergentu, D.-C.; Stein, C. J.; Ungur, L.; Vacher, M.; Valentini, A.; Veryazov, V. Modern Quantum Chemistry with [Open]Molcas. *J. Chem. Phys.* **2020**, *152*, 214117.